

Gallium Nitride-based Materials as Promising Catalysts for CO₂ Reduction: A DFT Study on the Effect of CO₂ Coverage and the Incorporation of Mg Doping or Substitutional In

Ida Ritacco,^[a] Matteo Farnesi Camellone,^{*[b]} Lucia Caporaso,^[a] Hermann Detz,^[c, d] and Valeria Butera^{*[c]}

[a] *I. Ritacco, L. Caporaso* Università degli Studi di Salerno Fisciano, Salerno 84084 (Italy)

[b] *M. Farnesi Camellone*
CNR-IOM Consiglio Nazionale delle Ricerche-Istituto Officina dei Materiali c/o SISSA
Trieste 34136 (Italy)
E-mail: farnesi@iom.cnr.it

[c] *H. Detz, Dr. V. Butera*
CEITEC – Central European Institute of Technology, Brno University of Technology
Brno 612 00 (Czech Republic)
E-mail: valeria.butera@ceitec.vutbr.cz

[d] *H. Detz*
Center for Micro- and Nanostructures & Institute of Solid State Electronics
TU Wien 1040 Vienna (Austria)

Abstract

Catalytic CO₂ conversion to fuels and chemicals is important for mitigating the climate change and reducing the dependence on fossil resources. In order to achieve this goal on a large industrial level, effective catalysts need to be developed. Among them, gallium nitride (GaN) and related Mg-doped and In-alloyed systems have been proven as efficient materials for the reduction of highly stable CO₂ molecules. This work presents a density functional theory (DFT) investigation, performing periodic boundary condition (PBC) calculations which allow to employ a more extended surface for a detailed analysis of the CO₂ coverage, and the effect of Mg doping and In alloying on the CO₂ adsorption and its conversion to CO.

The results show the great potential of GaN(100) surfaces to simultaneously bind and strongly activate multiple CO₂ molecules, which is a crucial aspect for an efficient CO₂ conversion process. Moreover, the presence of Mg-dopant on the top layer is found to be more beneficial for the CO₂ adsorption and activation with respect to both the pristine and In-alloyed system, and this effect is further improved by the inclusion of a second impurity on the top layer. In line with the previous experimental findings, these calculations support the potential of pristine GaN(100) to catalyze the CO₂-to-CO reduction. The results presented here offer crucial information for the development of more efficient and selective catalysts for the CO₂ reduction.

Introduction

CO₂ is considered the main culprit for global warming.^[1,2] Both large, industrial point sources, as well as small, mobile sources contribute with comparable amounts of CO₂ emissions. One potential way to reducing its emission below critical levels is the development of novel scientific approaches to capture CO₂ and to enable its conversion as a waste product into value-added products.^[3–8,9–11] Both the fields of homogeneous and heterogeneous catalysis have been extensively explored,^[12–19] and several catalysts have been reported experimentally to efficiently convert CO₂ into chemicals and fuels. In this regard, density functional theory (DFT) investigations can lead to an in-depth understanding of the structure/property relationship, and therefore contribute to the development of highly selective and efficient catalysts.^[20–23]

Among the promising catalysts reported in literature, we have addressed our attention to the thermodynamically stable wurtzite gallium nitride (GaN), which has shown unique electronic and optical properties^[24,25] Like other III-V semiconductor materials, the III-N family provides two ways to tune the material properties depending on the applications' requirements: the incorporation of

donor or acceptors^[26–30] and the formation of substitutional alloys using isovalent In or Al.^[27,31,32] These degrees of freedom were shown to have a significant influence on the efficiency of CO₂ reduction in experiments. In one of their works, AlOtaibi and co-workers^[33] report that the photochemical reduction of CO₂ to CH₃OH, CO, and CH₄ can be achieved on the pristine GaN(100), while a nearly 50-fold increase of the CO₂ conversion rate is obtained by the incorporation of Mg doping. Moreover, In_xGa_{1-x}N has been also proposed as highly promising photocatalysts for solar fuel applications, including the CO₂-to-CO and hydrocarbons, in solutions with a wide pH range.^[34–42] Motivated by these promising results, in a preliminary work,^[24] we have investigated the photocatalytic activity of the undoped GaN and GaN doped with one single Mg atom, along with the CO₂ reduction to methanol. The DFT investigation was carried out using a cluster model approach, that has some advantages over periodic boundary condition (PBC) calculations such as the utilization of hybrid functionals,^[43–45] and the investigation of complex reaction mechanism,^[46,47] at lower computational cost than periodic boundary condition (PBC) calculations. However, cluster model approaches do not allow for the investigation of

extended surfaces and heterojunctions, which can be more conveniently performed by means of PBC calculations.^[48–50] Therefore, the two use of the two methods is complementarity and crucial for a detailed understanding of the structure– property relationship.^[51]

Based on these considerations, in this work, we further extend our DFT investigation performing PBC calculations, and employing a more extended GaN(100) surface which includes six bilayers. This allows us to explore the surface CO₂ coverage, by considering the adsorption of one to nine CO₂ molecules on the pristine GaN(100) surface. Effects due to the incorporation of Mg or In are further investigated by considering up to eight different incorporation sites for these elements. After having identified the most stable doping/substitutional sites, we have eventually evaluated the influence of Mg dopant and In content on the CO₂ adsorption by replacing two and three Ga atoms with Mg and In, respectively. Eventually, we have investigated the reaction mechanism involved in the CO₂ conversion to CO, which is one of the main products observed experimentally along with CH₃OH, and CH₄. It is worthy to mention that a detailed investigation of the CO₂ conversion to methanol and CH₃* (and dimethyl ether) on pristine GaN materials has been already investigated in ref. [19 and 48]. In order to get a direct comparison with the previously reported results, we have focused on the CO₂-to-CO reduction reaction, occurring by the

direct breaking of the C–O bond upon CO₂ adsorption and activation. On the other hand, it is well-known that hydrogen evolution reaction^[52–54] represents a competing reaction in the CO₂ photoreduction to hydrocarbons. Future work will address the investigation of this potential side-reaction occurring on GaN-based materials.

The outcomes of this study complement our preliminary work based on cluster models, and contribute to shed light on the properties of Mg:GaN and In_xGa_{1-x}N materials as promising photocatalysts for CO₂ reduction.

Results and Discussion

In this study we employ the formalism of DFT to investigate the interaction between CO₂ and the GaN(100) surface at different CO₂ coverages (Section “CO₂ adsorption and coverage on pristine GaN(100)”), and the structural and electronic properties of Mg:GaN and In_xGa_{1-x}N materials (Section “Mg and In doping/ alloying”) as promising photocatalysts to promote CO₂ reduction. The charge rearrangement induced by the adsorption of CO₂ and/or by the inclusion of Mg and In elements on the GaN(100) surface is analyzed in terms of Bader charges as discussed in Section “Bader Charge Analysis”, while a detailed analysis of the projected density of states (PDOS) and spin densities are reported in Section S1 of the Supplementary Information (SI). Details about the activation barriers leading to the CO production are discussed in Section “CO₂ reduction to CO”.

For the sake of simplicity, the structures discussed throughout the text are labelled as NM_{site_x-y-z}-GaN + mads*, where N refers to the number of impurities, M refer to

the type of impurities (M = Mg, In), x, y and z refer to their incorporation sites and ads* refers to the m species (CO₂, CO and O) adsorbed on the surface.

CO₂ adsorption and coverage on pristine GaN(100)

Single CO₂ adsorption. As first step of our DFT study, we have determined the preferred adsorption mode of a single CO₂ molecule on the pristine GaN(100) surface.

Several adsorption modes have been investigated and the most favored (GaN+CO₂*) is shown in Figure 1, whose adsorption energy [computed according to Equation (1) in Computational Details] corresponds to – 1.50 and –1.27 eV, with and without including the van der Waals (vdW) interactions, respectively.

As shown in Figure 1, the CO₂ coordinates to the GaN(100) surface by forming one bond between the C atom of the CO₂ molecule and the N1 of the GaN(100) surface (C–N1, 1.41 Å), and two bonds among the oxygen atoms of the CO₂ molecule and the Ga atoms of the surface, (O1–Ga1 and O2–Ga2, whose calculated bond distances are 2.12 and 2.29 Å, respectively). Moreover, the O–C–O angle changes from 180° in the linear free gas-phase molecule to a 127.4°. The inclusion of the vdW corrections does not have any significant influence on the calculated parameters, which are reported in Table 1. Furthermore, the geometric parameters computed in this work are very similar to those obtained previously using a cluster model approach,^[24] and calculated by AlOtaibi and coworkers^[33] using PBC calculations with the optB86 exchange functional and including van der Waals interactions (see Table 1). Even though the CO₂ adsorption energy calculated in this work is 0.78 (0.55 with vdW) and 0.49 (0.26 with vdW) eV more positive than that computed in Ref. [24] and [33], respectively, all the studies support this adsorption mode as the most favored one.

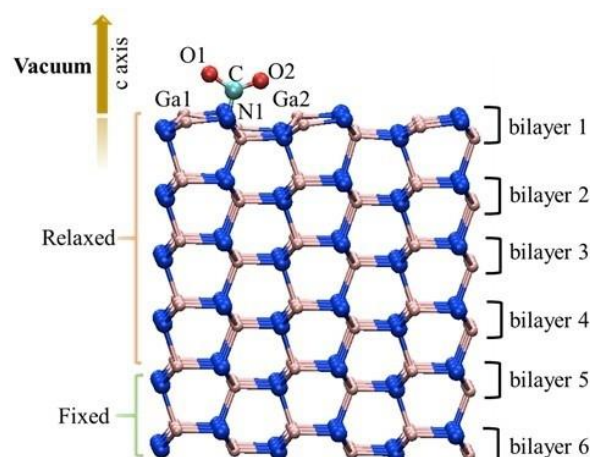


Figure 1. Side view of the optimized structure GaN + CO₂* of the most stable CO₂ adsorption mode on the GaN(100) surface. Ga, N, C and O atoms are represented in ball and sticks and depicted in pink, blue, cyan and red, respectively.

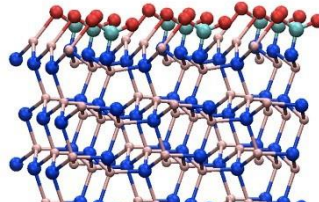
Table 1. CO₂ adsorption energies (E_{ads}) corresponding to the most favored adsorption mode, along with the main calculated geometric parameters. Values taken from Ref. [24] and Ref. [33] are also shown.

	This work no-vdW	vdW	Ref. [24]	Ref. [33]
E_{ads} [eV]	-1.27	-1.50	-2.05	-1.76
C-N1 [Å]	1.41	1.41	1.42	1.41
O1-Ga1 [Å]	2.12	2.10	2.32	2.24
O2-Ga2 [Å]	2.29	2.35	2.08	2.10
Ga1-N1-Ga2 [°]	167.3	167.6	167.0	-
O1-C-O2 [°]	127.4	127.6	127.4	128.3

CO₂ coverage. The influence of higher CO₂ coverage on the adsorption energy on the bare GaN(100) surface has been also evaluated. In this regard, the number of the CO₂ molecules has been progressively increased from one (1/9 ML, *single CO₂ adsorption*, described above) to nine molecules (1 ML, full coverage, displayed in the inset of Table 2). In this case, only the most favorable adsorption mode obtained with one CO₂ molecule has been considered. The corresponding adsorption energies are reported in Table 2, while the optimized structures are shown in Section S2 of the SI.

As it can be seen from Table 2, the inclusion of vdW interactions leads to adsorption energies which are 0.23–0.27 eV more negative than those calculated without including vdW. On the other hand, the two different computational approaches lead to very similar energy trends and to optimized structures which show identical adsorption modes. For these reasons, only the results without including vdW forces will be discussed below, and they will be not included in our further investigation. The adsorption of CO₂ molecules implies that the top layer of the GaN(100) surface is partially distorted with a consequent rearrangement of the Ga–N bonds and Ga–N–Ga angles. On the other hand, new O–Ga and C–N bonds (whose calculated bond distance range from 2.00 to 2.30, and from 1.40 to 1.42 Å, respectively) are formed between the adsorbed CO₂ molecules and the surface Ga atoms. The balance between the distortion/interaction effects leads to little differences (falling in the range of the DFT error)

Table 2. CO₂ adsorption energies, $E_{\text{ads}}(m \text{ CO}_2)$ ($m = 1-9$, ML = 1/9-1), as function of the coverage, computed according to Equation (1) with and without including van der Waals interactions. Values are given in eV. Inset: Optimized structure, GaN + 9CO₂^{*}, of 9 CO₂ molecules on GaN (100) surface. Ga, N, C and O atoms are represented in ball and sticks and depicted in pink, blue, cyan and red, respectively.



m	ML	no vdW	vdW	m	ML	no vdW	vdW
1	1/9	-1.27	-1.50	6	2/3	-1.08	-1.35
2	2/9	-1.30	-1.53	7	7/9	-1.13	-1.39
3	1/3	-1.21	-1.46	8	8/9	-1.13	-1.39
4	4/9	-1.20	-1.44	9	1	-1.12	-1.39
5	5/9	-1.12	-1.37				

in the calculated CO₂ adsorption energies as a function of the CO₂ coverage. These results show that all the surface N atoms can act as active sites and strongly bind to one CO₂ molecule, even when the full CO₂ coverage (1 ML) is considered (see the inset in Table 2). Therefore, the capability of GaN to coordinate and activate CO₂ via C–N bonds is not hindered by the increase of the number of CO₂ molecules.

The formalism of *ab initio* thermodynamics has been employed to investigate the thermodynamic stability of different surfaces in the presence of different coverages of CO₂ molecules. The computed surface free energies of the GaN(100) surfaces with CO₂ molecules adsorbed at different coverage are shown in Figure 2. Our calculations predict that the stoichiometric GaN(100) surface and the surface with two adsorbed CO₂ molecules (GaN + 2CO₂^{*}) are the lowest energy structures for $m_{\text{CO}_2}(T,p) < -1.3$ and $-1.3 < m_{\text{CO}_2}(T,p) < -1.1$, respectively. The surface with full CO₂ coverage (GaN + 9CO₂^{*}) is the lowest energy structure for $m_{\text{CO}_2}(T,p) > -1.1$ eV. It turns out that this surface structure is thermodynamically stable in a wide range of temperatures T and pressures p that are relevant for applications in the realm of catalysis. These results further support those discussed above, underlying the great potential of this material as catalyst for CO₂ reduction.

Mg and In doping/alloying

In the following, we address two relevant strategies to explore how material properties can be tuned to increase the efficiency of CO₂ reduction processes. First, doping with Mg, which is a common acceptor in GaN technology.^[26,27] Second, the addition of isovalent In to form In_xGa_{1-x}N alloys.^[27,31]

Mono Doping/Alloying sites. The effect of doping/alloying with one Mg and In atom on the surface and “bulk-like” bilayers has been studied, by replacing one Ga atom with Mg or In at each layer. We did not include the last two layers since those

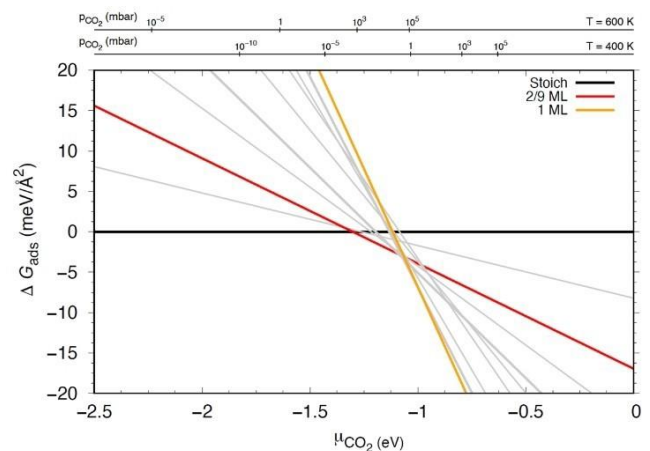


Figure 2. Surface free energies $\Delta G_{\text{ads}}(T,p)$ of the GaN(100) surfaces covered with a different number of CO₂ molecules as a function of the chemical potential of CO₂ $m_{\text{CO}_2}(T,p)$.

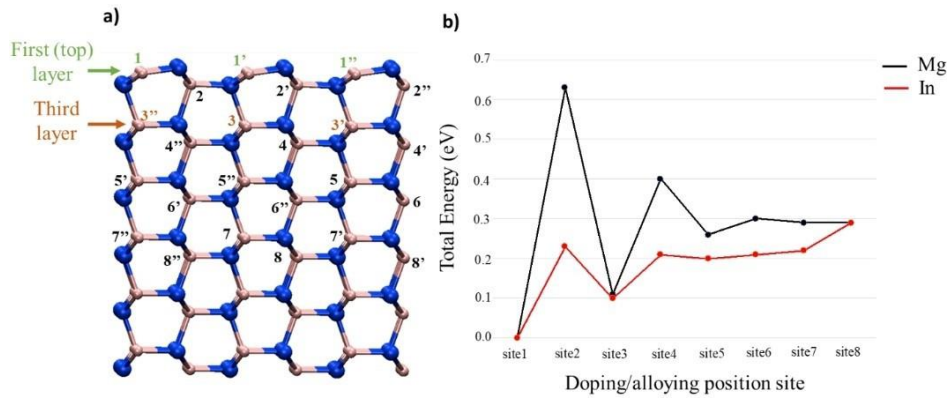


Figure 3. a) Eight different Mg/In incorporation sites labeled from 1 to 8. The two most stable sites “1” (located on the first or top layer) and “3” (located on the third layer) are highlighted; b) plot of the Ga-substitutional Mg (black line) and In (red line) sites as a function of the energy differences (with respect to the most stable site “1”).

are fixed in our calculations. Due to the periodic boundary conditions, all the Ga atoms in each layer are equivalent, and, therefore, any of them can be replaced. Figure 3 shows the eight different investigated incorporation sites, along with the plot of the corresponding energy differences relative to the most stable site. Our calculations show that the most stable structures (which will be referred as $M_{\text{site1}}\text{-GaN}$, with $M = \text{Mg, In}$) are obtained when both Mg and In impurities replace one Ga atom of the surface on site “1”. Site “3” is also accessible since it requires a higher energy of only ~ 0.10 eV with respect to site “1”. On the other hand, energy differences of 0.20- 0.40 eV are calculated for all the “bulk-like” incorporation sites (from “4” to “8”). Mg-doping at sites “2” leads to the less stable energy

structure, with an energy difference of 0.63 eV with respect to site “1”, while the corresponding energy for the In structure is similar to those calculated for the inner bulk-like sites. The stability of the selected systems was evaluated by calculating their binding energy per atom, as reported in Section S8 of the SI.

Single CO₂ Adsorption on Mono Doped/Alloyed systems.

When CO₂ is adsorbed on $M_{\text{site1}}\text{-GaN}$ ($M_{\text{site1}}\text{-GaN} + \text{CO}_2^*$ in Figure 4a) the newly formed Mg1–O1 bond becomes 0.11 Å longer than the corresponding Ga1–O1 calculated for the pristine GaN(100) case, while a much shorter Ga2–O2 bond distance of 2.04 Å is calculated. According to the Bader charges’ analysis, the replacement of the surface Ga³⁺ (Ga1) with Mg²⁺ (Mg1) determines an enhanced charge transfer from the surface to the adsorbed CO₂ molecule, and the establishment of a weaker Coulombic interaction between the divalent cation Mg²⁺ (Mg1) and the negatively charged oxygen atom (O1) and a stronger Coulombic interaction between the trivalent cation Ga³⁺ (Ga2) and the negative charged O2, as underlined by the elongation and shortening of Mg1–O1 and Ga2–O2 bonds, respectively. The corresponding adsorption energy of CO₂ on $M_{\text{site1}}\text{-GaN}$ is -2.13 eV, which is 0.86 eV more negative with respect to the non-doped case. All the geometric parameters and adsorption energies are listed in Table 3 and 4, respectively.

As seen for the CO₂ adsorption on pristine GaN(100) surface, also for the mono-doped Mg:GaN case, the calculated adsorption energy value is more positive than that calculated in Ref.^[24] (-2.48 eV) and Ref.^[24] (-3.12 eV).

Nevertheless, the energy differences between the CO₂ adsorption energy on the stoichiometric GaN(100) and on the mono-doped Mg:GaN (with

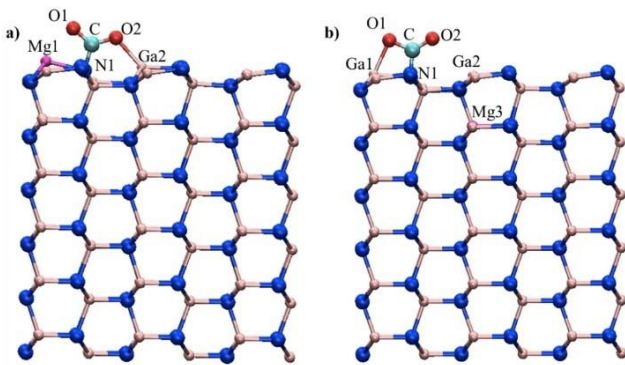


Figure 4. Side view of the optimized structures of a) $M_{\text{site1}}\text{-GaN} + \text{CO}_2^*$ (CO₂ adsorption on $M_{\text{site1}}\text{-GaN}$) and b) $M_{\text{site3}}\text{-GaN} + \text{CO}_2^*$ (CO₂ adsorption on $M_{\text{site3}}\text{-GaN}$). Ga, N, C, O and Mg atoms are represented in ball and sticks and depicted in pink, blue, cyan, red and magenta, respectively

2

	$M_{\text{site1}}\text{-GaN} + \text{CO}_2^*$	$2M_{\text{site1-1}}\text{-GaN} + \text{CO}_2^*$	$\text{In}_{\text{site1}}\text{-GaN} + \text{CO}_2^*$	$2\text{In}_{\text{site1-1}}\text{-GaN} + \text{CO}_2^*$	$M_{\text{site1}}\text{In}_{\text{site1}}\text{-GaN} + \text{CO}_2^*$
C–N1 (Å)	1.40	1.41	1.40	1.40	1.40
O1–M1 (Å)	2.23	2.10	2.32	2.25	2.13
O2–Ga2/M2(Å)	2.04	2.05	2.11	2.25	2.19
M1–N1–Ga2/M2 (°)	164.1	161.7	166.1	164.8	162.6
O1–C–O2 (°)	124.6	126.3	124.5	122.8	123.2

Table 4. CO ₂ adsorption energies (E_{ads}) on M _{site1} -GaN, M _{site3} -GaN, 2M _{site1-1'} -GaN, 3M _{site1-1'-1''} -GaN (M =Mg, In). Values are given in eV.					
E_{ads}	Mg _{site1} -GaN + CO ₂ *	Mg _{site3} -GaN + CO ₂ *	2Mg _{site1-1'} -GaN + CO ₂ *	2Mg _{site1-3'} -GaN + CO ₂ *	3Mg _{site1-1'-1''} -GaN + CO ₂ *
	-2.13	-1.22	-2.55	-1.93	-2.52
E_{ads}	3Mg _{site1-1'-1''} -GaN + 2CO ₂ *	In _{site1} -GaN + CO ₂ *	In _{site3} -GaN + CO ₂ *	2In _{site1-1} -GaN + CO ₂ *	Mg _{site1} In _{site1} -GaN + CO ₂ *
	-2.33	-1.71	-1.22	-2.00	-2.53

Mg replacing a surface Ga atom) are very similar and correspond to 0.86, 0.72 and 1.07 eV for the calculations presented here, those reported in Ref.[33] and Ref.[24] respectively. Moreover, the adsorption energy of CO₂ on Mg_{site3}-GaN (in which Mg replaces a Ga atom on site “3”, Mg_{site3}-GaN+CO₂* in Figure 3b) is calculated to be -1.22 eV, which is 0.91 eV more positive than that calculated for CO₂ adsorbed on Mg_{site1}-GaN, and very similar to that computed for the CO₂ adsorption on the bare GaN(100) surface, underlying that the presence of the Mg dopant on the top layer notably favors the CO₂ adsorption. By using a cluster model approach, similar trends have been computed.^[33] Indeed, the adsorption energy of CO₂ adsorbed on the GaN(100) cluster model that includes a Mg atom in site “3” (-2.29 eV) is 0.83 eV more positive than that including a Mg atom in site “1”(-3.12 eV) and very similar to that calculated for the pristine GaN(100) cluster model (-2.05 eV).

These results show that, besides the diverse absolute values of the adsorption energies calculated using different computational methods and protocols, similar trends are computed, and all the approaches confirm that the presence of a Mg-dopant on the surface is beneficial for the adsorption of CO₂, leading to the strongest (most negative) adsorption energies.

Replacing the Mg dopant on site “1” with In disfavors the CO₂ adsorption on In_{site1}-GaN of 0.42 eV. The more positive adsorption energy calculated for In_{site1}-GaN+ CO₂* is explained by the further elongation of 0.09 and 0.07 Å of O1-In1 and O2-Ga2 bonds, respectively, in comparison with the corresponding bonds in Mg_{site1}-GaN+CO₂*. Therefore, weaker interactions are established underlying a lower capability of the In

atom to activate the CO₂ molecule. On the other hand, the same adsorption energy of -1.22 eV is computed when CO₂ is adsorbed on Mg_{site3}-GaN and In_{site3}-GaN, which further confirms the major influence of the surface doping/alloying on the CO₂ adsorption. The relative optimized structures of In_{site1}-GaN+CO₂* and In_{site3}-GaN+CO₂* are shown in Section S3 of the SI.

Doping/Alloying Concentration Influence on CO₂ adsorption. Since our calculations have shown the importance of surface doping/alloying, the effect of impurities concentration has been evaluated by replacing two and three surface Ga atoms as shown in Figure 5a and 5b, respectively. Omitting the fixed GaN layers at the bottom, the impurities were placed within the four top-most layers. A maximum amount of three impurities within these structures, corresponds to a concentration of 4 %, which is a realistic value for both, strained InGaN on GaN, as well as for highly doped Mg:GaN.^[55] According to our calculations, the inclusion of the second Mg dopant as in 2Mg_{site1-1'}-GaN+CO₂* (Figure 5a) leads to a CO₂ adsorption energy which is 0.42 eV more negative with respect to the mono-doped Mg:GaN (Mg_{site1}-GaN+CO₂*) discussed above. Indeed, the presence of the second surface Mg atom, leads to an additional Mg2-O2 interaction, whose calculated distance is 2.05 Å. Moreover, the Mg1-O1 bond is also calculated to be 0.12 Å shorter than the mono-doped Mg:GaN case. Bader charges’ analysis (see the next paragraph and Section 5 of the SI) underlines that both O1 and O2 atoms bear a more negative charge with respect to the mono-doped and bare GaN cases, implying stronger Coulombic Mg/O interactions which are responsible of the shortening of these two Mg-O bonds. Therefore, thanks to those stronger interaction a more stable structure is obtained. On the other

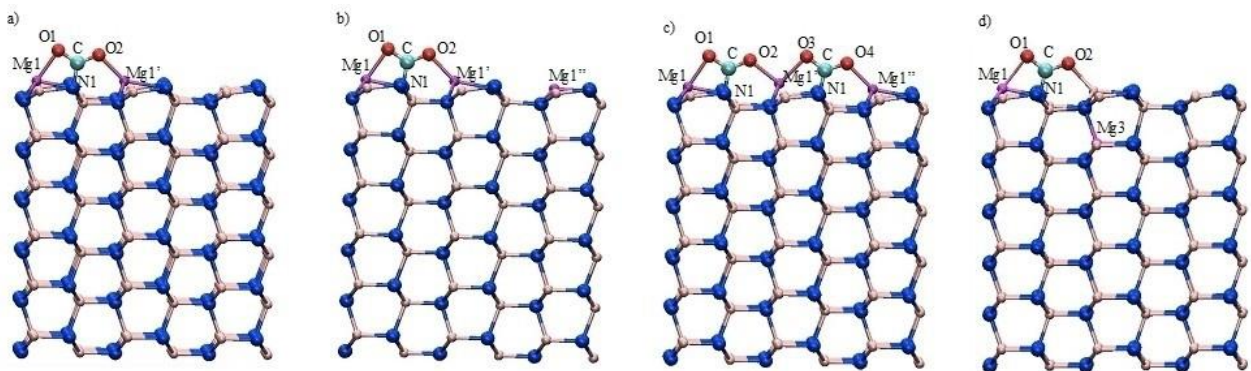


Figure 5. Side view of the optimized structures of a) 2Mg_{site1-1'}-GaN + CO₂* (two Mg dopants on the top layer); b) 3Mg_{site1-1'-1''}-GaN + CO₂* (three Mg dopants on the top layer); c) 3Mg_{site1-1'-1''}-GaN + 2CO₂* (three Mg dopants on the top layer); d) 2Mg_{site1-3'}-GaN + CO₂* (two Mg dopants on the top and second bilayer, respectively). Ga, N, C, O and Mg atoms are represented in ball and sticks and depicted in pink, blue, cyan, red and magenta, respectively.

hand, introducing a third surface Mg dopant, as in $3\text{Mg}_{\text{site}1-1'-1''}\text{-GaN}+\text{CO}_2^*$ (Figure 5b) has no consequence on the calculated adsorption energy (and the calculated Mg–O bond distances), since the third Mg atom is too far from the CO_2 and it cannot be involved in further interactions to stabilize the resulting structure. Nevertheless, the presence of the third surface Mg- dopant favors the adsorption of a second CO_2 molecule (see Figure 5c) leading to an adsorption energy per CO_2 molecule of -2.33 eV, which is 1.23 eV more negative than that on the pristine GaN(100) (see Table 2). Eventually, to further confirm the beneficial effect of the surface Mg-doping, we investigated the adsorption of CO_2 on $2\text{Mg}_{\text{site}1-3'}\text{-GaN}$ ($2\text{Mg}_{\text{site}1-3'}\text{-GaN}+\text{CO}_2^*$ in Figure 5d), in which two Mg dopants are present and occupy site “1” and site “3”, respectively. The calculated adsorption energy is -1.93 eV, which is 0.62 less favored than that of $2\text{Mg}_{\text{site}1-1'}\text{-GaN}+\text{CO}_2^*$. Interestingly, the addition of a second Mg dopant in the inner layer, as in $2\text{Mg}_{\text{site}1-3'}\text{-GaN}+\text{CO}_2^*$, disfavors of 0.17 eV the CO_2 adsorption with respect to the mono-doped case $\text{Mg}_{\text{site}1}\text{-GaN}$. All those results convey to demonstrating that only surface Mg-doping is beneficial for the CO_2 adsorption and activation.

We have eventually considered the influence of increasing In dopant’s concentration on the CO_2 adsorption. Based on the results discussed above for the Mg-doped systems, only the most favored CO_2 adsorption on $2\text{In}_{\text{site}1-1'}\text{-GaN}$ has been considered ($2\text{In}_{\text{site}1-1'}\text{-GaN}+\text{CO}_2^*$ shown in Figure S7 of the SI). Table 3 reports the geometric parameters calculated for CO_2 on $2\text{Mg}_{\text{site}1-1'}\text{-GaN}$ and $2\text{In}_{\text{site}1-1'}\text{-GaN}$. Even though very similar C–O and C–N bond distances are computed for both the doped/ alloyed systems, shorter M–O bonds between M and O atoms of the adsorbed CO_2 are calculated for the Mg-doped system with respect to In. Thanks to those stronger interactions, the adsorption energy of CO_2 on $2\text{Mg}_{\text{site}1-1'}\text{-GaN}$ is 0.55 eV more negative than that of $2\text{In}_{\text{site}1-1'}\text{-GaN}+\text{CO}_2^*$.

Eventually the coexistence of Mg doping and In alloying has been investigated by replacing two Ga atoms with Mg and In elements at the site 1 and 1', respectively. The simultaneous doping/alloying does not have significant influence on the CO_2 adsorption mode in comparison with the doping and alloying separately. Indeed, as depicted from Figure S8 of the SI, the CO_2 molecule bends upon absorption changing the O1–C–O2 angle to 123.2° . The calculated adsorption energy is very similar to the $2\text{Mg}_{\text{site}1-1'}\text{-GaN}+\text{CO}_2$ case, and 0.53 more negative than that calculated for the $2\text{In}_{\text{site}1-1'}\text{-GaN}$ system. These results suggest Mg-doping/In-alloying has also the potential for enhancing the CO_2 adsorption.

Bader charge analysis

To further describe the adsorption characteristic of CO_2 on pristine and doped GaN, charge analysis has been performed following the Bader’s theory, since the charge enclosed within the Bader volume can be considered a good approximation of the total electronic charge of an atom.^[56–58]

Table 5 reports the sum of the Bader charges ($\sum q$, e^-) of the free CO_2 and CO_2 adsorbed on the pristine, Mg- and In-GaN. Only the most stable adsorption modes are reported. Δq represents the difference between the Bader charges of the gas phase and coordinated CO_2 , calculated according to Equation (3) (see “Computational Details” section).

More details about the calculated Bader charges of all the atoms involved in the interactions between the pristine, Mg- and In-GaN and CO_2 are reported in Table S1 of the SI.

The difference between the Bader charges of the free and adsorbed CO_2 molecule on GaN and M-GaN (M=Mg, In), clearly underlines a charge transfer from the surface to the molecule which is more marked when Mg-doped system are considered. Similar results were obtained by AlOtaibi and co-workers,^[33] who calculated an electron-charge increase of 0.3947 and 0.4785 e on the CO_2 molecule on the bare GaN and mono doped Mg:GaN (analogues to $\text{Mg}_{\text{site}1}\text{-GaN}+\text{CO}_2^*$), respectively, implying a more surface-mediated charge transfer in presence of Mg.

On the other hand, our calculations show that the presence of two In dopants ($2\text{In}_{\text{site}1-1'}\text{-GaN}+\text{CO}_2^*$) does not contribute to an improvement of the surface charge transfer to the CO_2 molecule with respect to the pristine GaN, and exactly the same values of Δq are obtained. Indeed, the shortest bond distances calculated for the doped Mg:GaN systems imply the strongest interactions between the adsorbed CO_2 and the surface, and therefore justify the highest charge transfer.

The co-existence of Mg and In as in $\text{Mg}_{\text{site}1}\text{In}_{\text{site}1'}\text{-GaN}+\text{CO}_2^*$ leads to an increase of charge transfer from the surface to the CO_2 molecule in comparison with the pristine GaN and $2\text{In}_{\text{site}1-1'}\text{-GaN}+\text{CO}_2^*$. Interestingly, in $\text{Mg}_{\text{site}1}\text{In}_{\text{site}1'}\text{-GaN}+\text{CO}_2^*$, the charge transfer to the adsorbed CO_2 is 0.11 e and 0.18 e lower than the mono- and di-Mg doped cases, respectively. These results on one side further support the beneficial effect of Mg in activating the adsorbed CO_2 via charge transfer, on the other side suggest that the replacement of Mg and Ga in position 1' by In worsens the surface charge transfer contribution.

CO_2 reduction to CO

Pristine GaN(100). Our results have shown that CO_2 molecule binds strongly to the pristine GaN(100) surface, and, upon the

Table 5. Bader charge analysis for the free and adsorbed CO_2 molecule on GaN and M-GaN (M=Mg, In). Only the most stable adsorption modes are reported.

	CO_2 (free)	$\text{GaN}+\text{CO}_2^*$	$\text{Mg}_{\text{site}1}\text{-GaN}+\text{CO}_2^*$	$2\text{Mg}_{\text{site}1-1'}\text{-GaN}+\text{CO}_2^*$	$2\text{In}_{\text{site}1-1'}\text{-GaN}+\text{CO}_2^*$	$\text{Mg}_{\text{site}1}\text{In}_{\text{site}1'}\text{-GaN}+\text{CO}_2^*$
$\sum q$	16.0	16.35	16.53	16.60	16.35	16.42
Δq	/	+0.35	+0.53	+0.60	+0.35	+0.42

adsorption, both the C–O bonds elongates and weakens significantly. This effect is enhanced for the O1–C bond as underlined by the calculated longer bond distance of 0.04 Å with respect to O2–C. We have, therefore, investigated the potential direct breaking of the O1–C bond leading to the formation of $\text{GaN} + \text{CO}^* \cdot \text{O}^*$, in which CO^* and O^* species are adsorbed on the GaN surface. In the corresponding optimized structure, the O1 adsorbed atom is bound to two surface Ga1 and Ga1' atoms with calculated distances of 1.84 and 1.99 Å, respectively, and the formed CO molecule binds to the nitrogen atom with a C–N1 bond of 1.24 Å, while the calculated O1–C distance is 2.94 Å. However, as shown in the potential energy surface of Figure 6a (black line), the $\text{GaN} + \text{CO}^* \cdot \text{O}^*$ is 0.49 eV above the reactants' asymptotes and its formation involves a calculated energy barrier of 1.96 eV.

As mentioned earlier, beside the production of CO, methanol is also obtained as alternative reaction product. The CO_2 reduction pathway to CH_3OH has been already investigated.⁴⁹ Due to the multi-step nature of the CH_3OH formation reaction, the energetic span model (ESM)^[59,60] has been applied, leading to a calculated δE connecting the rate-determining intermediate (TDI)

and the rate-determining transition state (TDTS) of 3.37 eV (3.70 eV using a cluster model approach^[24]). These results underline that the direct breaking of one C–O bond of the CO_2 molecule adsorbed on the pristine GaN surface is largely preferred than the CO_2 hydrogenation to methanol, in line with the experimental findings which underline that the reduction of CO_2 to CO dominates on as-grown GaN nanowires under ultraviolet light irradiation and a significant amount of CO (~ 1130 $\mu\text{mol gcat}^{-1}$), has been measured from the as-grown GaN nanowires.^[61] However, the very high calculated energy barriers, for both CO and methanol production, support the need of photoactivating the reaction via UV-visible light.

Mg-doped. In order to determine the influence of the Mg in the CO_2 -to-CO conversion, we have calculated the activation barrier for the reaction on $\text{Mg}_{\text{site1}}\text{-GaN}$.

Interestingly, the energy barrier involved in the O1–C bond breaking is 0.40 eV higher than that calculated on the pristine GaN surface. As Figure 6a shows, this difference is mainly due to the much lower energy at which the $\text{Mg}_{\text{site1}}\text{-GaN} + \text{CO}_2^*$ intermediate lies with respect to the analogous $\text{GaN} + \text{CO}_2^*$ in reference to the separated reactants. In order to better understand

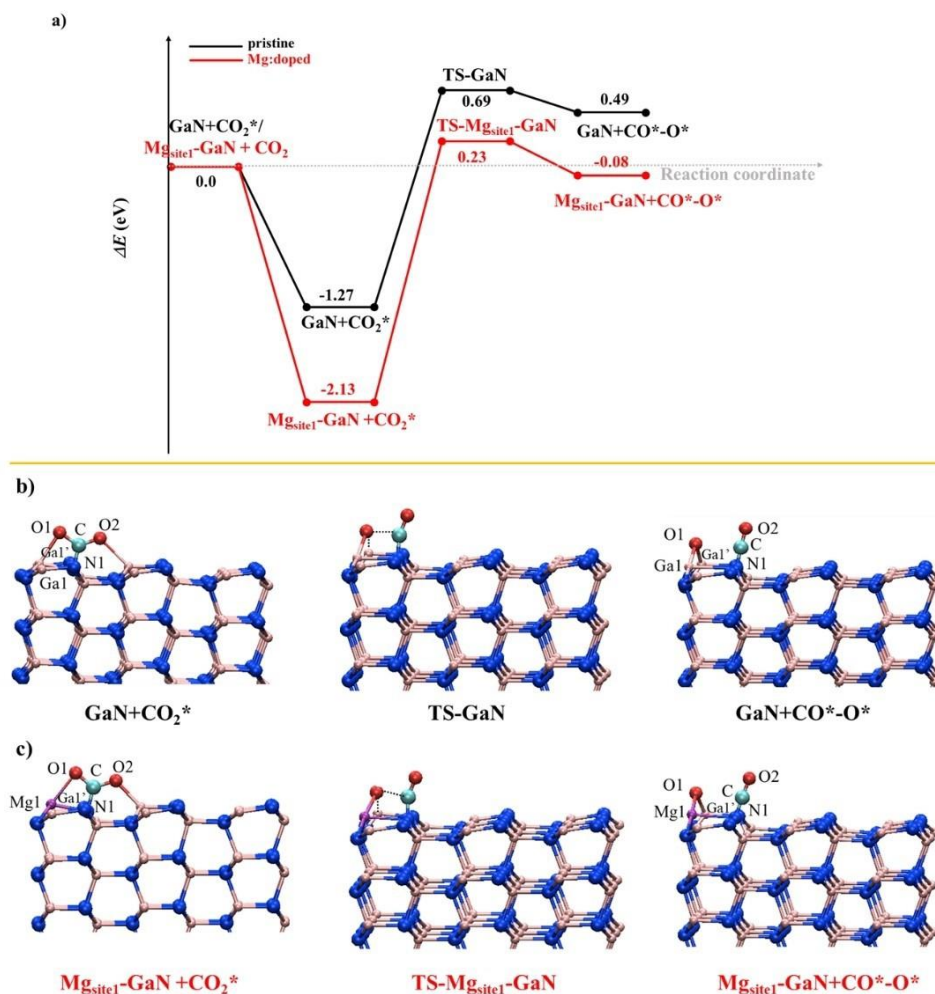


Figure 6. (a) Calculated energy profile for the CO_2 -to-CO conversion on pristine GaN(100) (black line) and $\text{Mg}_{\text{site1}}\text{-GaN}$ (red line). Energies are in eV and relative to the asymptote of the reactant. Optimized structures of the intercepted stationary points along b) pristine and c) Mg-doped pathway.

which contributions are mainly involved in the stabilizing those intermediates, we have decomposed the corresponding adsorption energies, into the two main contributions, which are the interaction, E_{INT} , and the distortion, E_{DIST} , energies, whose details are discussed in Section S6 of the SI. Our results show very positive distortion energies of 3.68 and 3.71 eV for the $GaN+CO_2^*$ and $Mg_{site1}-GaN+CO_2^*$, respectively, with a significant contribution associated to the distortion of the adsorbed CO_2 molecule (2.64 and 2.88 eV), that support a similar capability of both the pristine and Mg-doped systems of activating the CO_2 upon adsorption. On the other hand, very negative values of -4.95 and -5.85 eV are calculated for the E_{INT} for the pristine and Mg-doped intermediate, respectively. The significant stronger interaction between CO_2 molecule and the surface in the $Mg_{site1}-GaN+CO_2^*$ intermediate, is therefore responsible for the higher activation energy required to break the C–O bond. Differently from the pristine case, the formation of the $Mg_{site1}-GaN+CO^*-O^*$ (shown in Figure 6c) is slightly exergonic of 0.08 eV with respect to the separated reactants, while the formation of $GaN+CO^*-O^*$ is a high endergonic process of 0.49 eV. Therefore, the thermodynamic can play a crucial role in the CO_2 -to-CO conversion catalyzed by GaN materials.

Conclusion

In this work, a DFT study based on PBC calculations has been carried out to evaluate how the increase of the CO_2 coverage influences its adsorption on GaN (100) surface, and to investigate the structural and electronic properties of Mg:GaN and $In_xGa_{1-x}N$ materials as promising photocatalysts to promote CO_2 reduction. Our calculations support the ability of stoichiometric GaN to adsorb and activate CO_2 molecule, and the corresponding adsorption energy is -1.50 and -1.27 eV, with and without including vdW interactions, respectively. Even though the CO_2 adsorption energy calculated in this work is 0.78 (0.55 with vdW) and 0.46 (0.26 with vdW) eV more positive than computed in previous works, all the studies support the analogous preferred adsorption mode.

Our results have also shown that all the surface N atoms can act as active sites and strongly bind to the carbon atom of the CO_2 molecule. Therefore, the presence of adsorbed CO_2 molecules does not hinder the coordination of further CO_2 molecules as soon as available N surface active sites are present. Moreover, the computed surface free energies of the GaN(100) surfaces with adsorbed CO_2 molecules at different coverage show that the surface with full CO_2 coverage (1 ML) is the most thermodynamically stable in a wide range of temperatures (T) and pressures (p) that are relevant for applications in the realm of catalysis. Therefore, those results support the great potential of GaN as catalyst for CO_2 reduction.

In order to explore the influence of doping on the bulk-like third and fourth bilayers, eight different doping sites have been considered for both Mg and In elements. Our calculations show that the most stable structures are obtained when the Mg dopant replaces one Ga atom of the top layer (site “1”).

However, Mg doping on the third layer (site “3”) requires a higher energy of only ~ 0.10 eV, and it can therefore be considered accessible for Mg-doping. Similar results have been obtained when the incorporation of In is considered.

Moving to the effect of the doping on the CO_2 adsorption, calculations reveal that replacing surface Ga^{3+} with Mg^{2+} enhances the charge transfer from the surface to CO_2 and its adsorption. In particular, the presence of one Mg-dopant on the top layer, as in $Mg_{site1}-GaN$, is beneficial for about 0.9 eV and this effect is further improved by the inclusion of a second impurity on the top layer ($2Mg_{site1-1'}-GaN$) with an additional stabilization of about 0.4 eV (~ -1.3 eV with respect the pristine GaN). In line with this result, when two surface Ga^{3+} are replaced with two In^{3+} , the charge transfer from the surface to the adsorbed CO_2 is lower than in the case with two Mg^{2+} . As matter of fact, the adsorption of CO_2 on the surface enhances of only 0.7 eV compared to the case of pristine GaN. On the other hand, the coexistence of Mg doping and In alloying has been investigated and our results suggest Mg-doping/In-alloying enhances the CO_2 adsorption, even though the charge transfer from the surface to the adsorbed CO_2 molecule is reduced in comparison with both the mono- and di-Mg doped cases.

Eventually, we have investigated the reaction pathway leading to the formation of CO molecule. According to our results, the formation of CO is favored than MeOH over the pristine GaN (100) surface. This result is in line with the experimental findings which underline that the reduction of CO_2 to CO dominates on as-grown GaN nanowires under ultraviolet light irradiation.

The results presented in our study shed light on the properties of Mg:GaN and $In_xGa_{1-x}N$ and pave the way for the development of GaN-based materials as promising photo-catalysts for CO_2 reduction.

Computational Details

DFT calculations have been performed within PBC using the Perdew-Burke-Ernzerhof (PBE) exchange-correlation functional based on the generalized gradient approximation (GGA),^[62] as implemented in the Quantum Espresso code.^[63]

The spin-polarized Kohn-Sham equations were solved in the plane-wave pseudopotential framework, with the wave function basis set and the Fourier representation of the charge density being limited by kinetic cutoffs of 50 and 400 Ry, respectively. The Ga, N, C, O, Mg and In atoms were described by ultrasoft pseudopotentials.^[64]

We built up the structural model for the GaN(100) surface as shown in Figure 1, which consists of 216 atoms.

Our choice of considering GaN(100) is motivated by a previous study in which the calculated surface energies revealed that GaN(100) surface is more stable than GaN(110) and GaN(001).^[65] Moreover, GaN(100) has also been used in Reference [24] and [33]. Our computed lattice parameters of the GaN bulk hexagonal unit cell are $a = 3.235$ Å and $c = 5.273$ Å, which are in good agreement with the experimental values ($a = 3.189$ Å and $c = 5.185$ Å).^[65] The GaN(100) surface has been modeled with periodic (3×3) supercell slabs consisting of six Ga N bilayer separated by more than 17 Å in the c direction perpendicular to the surface. The final dimensions of the GaN(100) 3×3 supercell are $a = 9.706$ Å, $b = 15.820$ Å, and $c =$

$c =$

31.943 Å. The threshold for energy convergence is set to 10^{-6} eV. The atoms in the lowest laying two Ga N bilayer were constrained to their equilibrium bulk like positions, while all the other atoms were free to move under the action of the interatomic forces. Due to the large dimension, Γ point have been used for the Brillouin zone integration.

The adsorption energies (E_{ads}) of the CO_2 molecules on the GaN(100) surfaces have been computed using Equation (1):

$$E_{\text{ads}} = \frac{1}{m} (E_{\text{GaN}(100)+m\text{CO}_2} - E_{\text{GaN}(100)} - mE_{\text{CO}_2})$$

where m is the number of adsorbed CO_2 molecules, $E_{\text{GaN}(100)+m\text{CO}_2}$ is the total energy of $m\text{CO}_2$ molecules adsorbed on the surface, while $E_{\text{GaN}(100)}$ and E_{CO_2} are the total energies of the stoichiometric GaN(100) surface and a CO_2 molecule, respectively.

Benchmark calculations have been performed in order to understand the role of van der Waals (vdW) interactions on the adsorption of CO_2 molecules on the GaN(100) surface. The zero damping DFT-D3 method of Grimme^[66] has been employed. The corresponding results suggest that the inclusion of vdW forces does not affect significantly the values of the adsorption energies.

In order to study the thermodynamic stability of different surfaces in the presence of CO_2 molecules we have employed the formalism of *ab initio* thermodynamics.^[67] We assume that the surfaces can exchange CO_2 molecules with a surrounding gas phase. If we assume that the system is in thermodynamic equilibrium, the most stable surface surfaces decorated with CO_2 molecules at a given temperature T and pressure p are given by the minimum of the surface Gibbs free energy. The Gibbs free energy is computed with Equation (2):

$$\Delta G_{\text{ads}}(T, p) = \frac{1}{A} \{ E_{\text{tot}}^{\text{CO}_2\text{-ads}}(N_{\text{CO}_2}) - [E_{\text{tot}}^{\text{slab-GaN}(100)} + \Delta N_{\text{CO}_2} \mu_{\text{CO}_2}(T, p)] \}$$

Where A is the surface area, $E_{\text{tot}}^{\text{CO}_2\text{-ads}}(N_{\text{CO}_2})$ is the energy of the surface covered with N CO_2 molecules, $E_{\text{tot}}^{\text{slab-GaN}(100)}$ is the energy of the clean GaN(100) slab, ΔN_{CO_2} is the difference in the number of CO_2 molecules between the two surfaces and, $\mu_{\text{CO}_2}(T, p)$ is the chemical potential representing the Gibbs free energy of the gas phase with which the CO_2 molecules are exchanged. We assume that volume and entropy contributions are negligible in $\Delta G_{\text{ads}}(T, p)$.^[67] Therefore, the Gibbs free energies are approximated by the total energies of our DFT calculations. The upper bound of the chemical potential of CO_2 $\mu_{\text{CO}_2}(T, p)$ is given by the total energy of CO_2 , E_{CO_2} . This upper bound is taken as the zero of our energy scale by using $\Delta \mu_{\text{CO}_2} = \mu_{\text{CO}_2}(T, p) - E_{\text{CO}_2}$.

Charge analysis has been performed following Bader's theory, since the charge enclosed within the Bader volume can be considered a good approximation of the total electronic charge of an atom.^[56-58] The differences between the Bader charges of the gas phase and coordinated CO_2 molecules, Δq , have been calculated according to Equation 3:

$$\Delta q = \sum q(\text{CO}_2 \text{ surface - bound}) + \sum q(\text{CO}_2 \text{ free})$$

Where $\sum q(\text{CO}_2 \text{ surface - bound})$ is the sum of the Bader charges of the CO_2 adsorbed on the pristine and M-GaN surface, and $\sum q(\text{CO}_2 \text{ free})$ is the sum of the free CO_2 .

The reaction paths for the CO_2 -to- CO conversion were investigated by means of the climbing image nudged elastic band (CI-NEB) method,^[68-70] and the corresponding activation barrier (E_a) is defined by Equation (4):

$$E_a = \frac{1}{4} (E_{\text{TS}} - E_{\text{IS}})$$

where E_{TS} and E_{IS} are the total energies of the transition state (TS) and the initial structure (IS), respectively, as defined in Section "CO₂ reduction to CO".

Supporting Information

Supporting Information is available from the Wiley Online Library or from the author. Supporting Information includes details about projected density of states (PDOS) of the undoped and Mg-, In-doped GaN(100) surface; optimized structures and adsorption energies (E , eV) of $m\text{CO}$ ($m = 1-9$, A to I) on GaN(100); optimized structure of the CO_2 adsorption on $\text{In}_{\text{site}1}\text{-GaN}$, $\text{In}_{\text{site}3}\text{-GaN}$, $\text{In}_{\text{site}1-1}\text{-GaN}$ and $\text{Mg}_{\text{site}1}\text{In}_{\text{site}1}\text{-GaN}$; calculated Bader charges of the atoms involved in the interactions between the pristine, Mg-, In-, Mg/In-GaN and CO_2 ; main contributions (E_{INT} and E_{DIST}) to the adsorption energy (E_{ads}).

Author Contributions

I.R. and V.B. performed the DFT simulations and analysed the data. V. B. wrote the manuscript. M.F.C. investigated the CO_2 coverages as a function of the CO_2 chemical potential. All the authors contributed to the manuscript.

Acknowledgements

I.R. thanks MIUR and European Union for AIM-International attraction and mobility call for researchers funded by PON RI 2014–2020. The Computational work was performed using the resources of the KAUST Super-computing Laboratory (KSL) at KAUST, and IT4Innovations National Supercomputer Center, supported by The Ministry of Education, Youth and Sports from the Large Infrastructures for Research, Experimental Development and Innovations Project "e-Infrastructure CZ – LM2018140". CzechNanoLab project LM2018110 funded by MEYS CR is gratefully acknowledged for the financial support at CEITEC Nano Research Infrastructure.

Conflict of Interest

The authors declare no conflict of interest.

Data Availability Statement

The data that support the findings of this study are available in the supplementary material of this article.

- [1] N. J. L. Lenssen, G. A. Schmidt, J. E. Hansen, M. J. Menne, A. Persin, R. Ruedy, D. Zyss, *J. Geophys. Res. [Atmos.]* **2019**, *124*, 6307–6326.
- [2] J. Hansen, R. Ruedy, M. Sato, K. Lo, *Rev. Geophys.* **2010**, *48*, 4004.
- [3] A. Goeppert, M. Czaun, G. K. Surya Prakash, G. A. Olah, *Energy Environ. Sci.* **2012**, *5*, 7833–7853.
- [4] R. M. Cuéllar-Franca, A. Azapagic, *J. CO₂ Util.* **2015**, *9*, 82–102.
- [5] M. Takht Ravanchi, S. Sahebdehfar, *Appl. Petrochem. Res.* **2014**, *4*, 63–77.
- [6] A. Goeppert, M. Czaun, R. B. May, G. K. S. Prakash, G. A. Olah, S. R. Narayanan, *J. Am. Chem. Soc.* **2011**, *133*, 20164–20167.
- [7] W. Zhou, K. Cheng, J. Kang, C. Zhou, V. Subramanian, Q. Zhang, Y. Wang, *Chem. Soc. Rev.* **2019**, *48*, 3193–3228.
- [8] T. Sakakura, J. C. Choi, H. Yasuda, *Chem. Rev.* **2007**, *107*, 2365–2387.
- [9] B. Zhou, X. Kong, S. Vanka, S. Cheng, N. Pant, S. Chu, P. Ghamari, Y. Wang, G. Botton, H. Cuo, Z. Mi, *Energy Environ. Sci.* **2019**, *12*, 2842–2848.
- [10] J. Kim, E. E. Kwon, *J. CO₂ Util.* **2019**, *33*, 72–82.
- [11] M. Qu, G. Qin, J. Fan, A. Du, Q. Sun, *Appl. Surf. Sci.* **2021**, *555*, 149652.
- [12] S. Wang, C. Xi, *Chem. Soc. Rev.* **2019**, *48*, 382–404.
- [13] J. R. Cabrero-Antonino, R. Adam, M. Beller, *Angew. Chem. Int. Ed.* **2019**, *58*, 12820–12838; *Angew. Chem.* **2019**, *131*, 12950–12968.
- [14] S. Kar, A. Goeppert, G. K. S. Prakash, *Acc. Chem. Res.* **2019**, *52*, 2892–2903.
- [15] Q. W. Song, Z. H. Zhou, L. N. He, *Green Chem.* **2017**, *19*, 3707–3728.
- [16] S. Samanta, R. Srivastava, *Mater. Adv.* **2020**, *1*, 1506–1545.
- [17] H. Rao, L. C. Schmidt, J. Bonin, M. Robert, *Nature* **2017**, *548*, 74–77.
- [18] K. Beydoun, G. Ghattas, K. Thenert, J. Klankermayer, W. Leitner, *Angew. Chem. Int. Ed.* **2014**, *53*, 11010–11014; *Angew. Chem.* **2014**, *126*, 11190–11194.
- [19] A. Fujishima, K. Honda, *Nature* **1972**, *238*, 37–38.
- [20] V. Butera, H. Detz, *Catal. Sci. Technol.* **2021**, *11*, 3556–3567.
- [21] V. Butera, H. Detz, *ACS Omega* **2020**, *5*, 18064–18072.
- [22] U. Guharoy, T. Ramirez Reina, S. Gu, Q. Cai, *J. Phys. Chem. C* **2019**, *123*, 22918–22931.
- [23] C. R. Kwawu, A. Aniygyei, D. Konadu, B. Y. Antwi, *Mater. Renew. Sustain. Energy* **2021**, *10*, 9.
- [24] V. Butera, H. Detz, *Mater. Chem. Front.* **2021**, *5*, 8206–8217.
- [25] V. Butera, H. Detz, *ACS Appl. Energy Mater.* **2022**, *5*, 4684–4690.
- [26] H. Amano, *Rev. Mod. Phys.* **2015**, *87*, 1133.
- [27] I. Akasaki, *Rev. Mod. Phys.* **2015**, *87*, 1119.
- [28] I. Akasaki, H. Amano, H. Murakami, M. Sassa, H. Kato, K. Manabe, *J. Cryst. Growth* **1993**, *128*, 379–383.
- [29] H. P. Maruska, D. A. Stevenson, J. I. Pankove, *Appl. Phys. Lett.* **2003**, *22*, 303.
- [30] H. Amano, M. Kito, K. Hiramatsu, I. Akasaki, *Jpn. J. Appl. Phys.* **1989**, *28*, L2112–L2114.
- [31] S. Nakamura, *Rev. Mod. Phys.* **2015**, *87*, 1139.
- [32] K. Osamura, S. Naka, Y. Murakami, *J. Appl. Phys.* **1975**, *46*, 3432.
- [33] B. Alotaibi, X. Kong, S. Vanka, S. Y. Woo, A. Pofelski, F. Oudjedi, S. Fan, M. G. Kibria, G. A. Botton, W. Ji, H. Guo, Z. Mi, *ACS Energy Lett.* **2016**, *1*, 246–252.
- [34] J. D. Beach, R. T. Collins, J. A. Turner, *J. Electrochem. Soc.* **2003**, *150*, A899.
- [35] K. Ohkawa, Y. Uetake, M. Velazquez-Rizo, D. Iida, *Nano Energy* **2019**, *59*, 569–573.
- [36] K. Aryal, B. N. Pantha, J. Li, J. Y. Lin, H. X. Jiang, *Appl. Phys. Lett.* **2010**, *96*, 052110.
- [37] D. Wang, A. Pierre, M. G. Kibria, K. Cui, X. Han, K. H. Bevan, H. Guo, S. Paradis, A. R. Hakima, Z. Mi, *Nano Lett.* **2011**, *11*, 2353–2357.
- [38] B. Alotaibi, H. P. T. Nguyen, S. Zhao, M. G. Kibria, S. Fan, Z. Mi, *Nano Lett.* **2013**, *13*, 4356–4361.
- [39] M. G. Kibria, H. P. T. Nguyen, K. Cui, S. Zhao, D. Liu, H. Guo, M. L. Trudeau, S. Paradis, A. R. Hakima, Z. Mi, *ACS Nano* **2013**, *7*, 7886–7893.
- [40] M. G. Kibria, S. Zhao, F. A. Chowdhury, Q. Wang, H. P. T. Nguyen, M. L. Trudeau, H. Guo, Z. Mi, *Nat. Commun.* **2014**, *5*, 1–6.
- [41] S. Yotsushashi, M. Deguchi, Y. Zenitani, R. Hinogami, H. Hashiba, Y. Yamada, K. Ohkawa, *Appl. Phys. Express.* **2011**, *4*, 117101.
- [42] M. Ebaid, D. Priante, G. Liu, C. Zhao, M. Sharizal Alias, U. Buttner, T. Khee Ng, T. Taylor Isimjan, H. Idriss, B. S. Ooi, *Nano Energy* **2017**, *37*, 158–167.
- [43] V. Butera, M. C. Toroker, *J. Phys. Chem. C* **2016**, *120*, 12344–12350.
- [44] V. Butera, M. C. Toroker, *Materials* **2017**, *10*, 480.
- [45] M. D'Arienzo, L. Gamba, F. Morazzoni, U. Cosentino, C. Greco, M. Lasagni, D. Pitea, G. Moro, C. Cepek, V. Butera, E. Sicilia, N. Russo, A. B. Muñoz-García, M. Pavone, *J. Phys. Chem. C* **2017**, *121*, 9381–9393.
- [46] V. Butera, N. Fukaya, J. C. Choi, K. Sato, Y. K. Choe, *Inorg. Chim. Acta* **2018**, *482*, 70–76.
- [47] V. Butera, Y. Tanabe, Y. Shinke, T. Miyazawa, T. Fujitani, M. Kayanuma, Y. K. Choe, *Int. J. Quantum Chem.* **2021**, *121*, e26494.
- [48] I. Ritacco, C. Imperato, L. Falivene, L. Cavallo, A. Magistrato, L. Caporaso, M. Farnesi Camellone, A. Aronne, *Adv. Mater. Interfaces* **2021**, *8*, 2100629.
- [49] I. Ritacco, O. Sacco, L. Caporaso, M. F. Camellone, *J. Phys. Chem. C* **2022**, *126*, 3180–3193.
- [50] W. Navarra, I. Ritacco, O. Sacco, L. Caporaso, M. Farnesi Camellone, V. Venditto, V. Vaiano, *J. Phys. Chem. C* **2022**, *126*, 7000–7011.
- [51] V. Butera, A. Massaro, A. B. Muñoz-García, M. Pavone, H. Detz, *Front. Chem.* **2021**, *9*, 651.
- [52] Y. Zhao, S. Zhang, R. Shi, G. I. N. Waterhouse, J. Tang, T. Zhang, *Mater. Today* **2020**, *34*, 78–91.
- [53] J. Greeley, T. F. Jaramillo, J. Bonde, I. Chorkendorff, J. K. Nørskov, *Nat. Mater.* **2006**, *5*, 909–913.
- [54] J. K. Nørskov, T. Bligaard, A. Logadottir, J. R. Kitchin, J. G. Chen, S. Pandelov, U. Stimming, *J. Electrochem. Soc.* **2005**, *152*, J23.
- [55] P. Kozodoy, H. Xing, S. P. DenBaars, U. K. Mishra, A. Saxler, R. Perrin, S. Elhamri, W. C. Mitchel, *J. Appl. Phys.* **2000**, *87*, 1832.
- [56] E. Sanville, S. D. Kenny, R. Smith, G. Henkelman, *J. Comput. Chem.* **2007**, *28*, 899–908.
- [57] J. Zhao, D. Wang, X. Long, Y.-Z. Lyu, M. Guo, O. Sha, W. Tang, E. Sanville, G. Henkelman, *J. Phys. Condens. Matter.* **2009**, *21*, 084204.
- [58] G. Henkelman, A. Arnaldsson, H. Jónsson, *Comput. Mater. Sci.* **2006**, *36*, 354–360.
- [59] S. Kozuch, S. Shaik, *Acc. Chem. Res.* **2011**, *44*, 101–110.
- [60] L. Falivene, S. M. Kozlov, L. Cavallo, *ACS Catal.* **2018**, *8*, 5637–5656.
- [61] B. Alotaibi, S. Fan, D. Wang, J. Ye, Z. Mi, *ACS Catal.* **2015**, *5*, 5342–5348.
- [62] J. P. Perdew, K. Burke, M. Ernzerhof, *Phys. Rev. Lett.* **1996**, *77*, 3865.
- [63] P. Giannozzi, O. Andreussi, T. Brumme, O. Bunau, M. Buongiorno Nardelli, M. Calandra, R. Car, C. Cavazzoni, D. Ceresoli, M. Cococcioni, N. Colonna, I. Carnimeo, A. Dal Corso, S. de Gironcoli, P. Delugas, R. A. Distasio, A. Ferretti, A. Floris, G. Fratesi, G. Fugallo, R. Gebauer, U. Gerstmann, F. Giustino, T. Gorni, J. Jia, M. Kawamura, H. Y. Ko, A. Kokalj, E. Küçükbenli, M. Lazzeri, M. Marsili, N. Marzari, F. Mauri, N. L. Nguyen, H. v. Nguyen, A. Otero-De-La-Roza, L. Paulatto, S. Poncé, D. Rocca, R. Sabatini, B. Santra, M. Schlipf, A. P. Seitsonen, A. Smogunov, I. Timrov, T. Thonhauser, P. Umari, N. Vast, X. Wu, S. Baroni, *J. Phys. Condens. Matter.* **2017**, *29*, 465901.
- [64] D. Vanderbilt, *Phys. Rev. B* **1990**, *41*, 7892.
- [65] C. Liu, J. Kang, Z. Q. Huang, Y. H. Song, Y. S. Xiao, J. Song, J. X. He, C. R. Chang, H. Q. Ge, Y. Wang, Z. T. Liu, Z. W. Liu, *Nat. Commun.* **2021**, *12*, 1–10.
- [66] S. Grimme, J. Antony, S. Ehrlich, H. Krieg, *J. Chem. Phys.* **2010**, *132*, 154104.
- [67] K. Reuter, M. Scheffler, *Phys. Rev. B* **2001**, *65*, 035406.
- [68] G. Henkelman, B. P. Uberuaga, H. Jónsson, *J. Chem. Phys.* **2000**, *113*, 9901.
- [69] D. Sheppard, P. Xiao, W. Chemelewski, D. D. Johnson, G. Henkelman, *J. Chem. Phys.* **2012**, *136*, 074103.
- [70] D. Sheppard, G. Henkelman, *J. Comput. Chem.* **2011**, *32*, 1769–1771.